Three-Dimensional Seismic Response of Humboldt Bay Bridge-Foundation-Ground System

Ahmed Elgamal[1]; Linjun Yan[2]; Zhaohui Yang[3]; and Joel P. Conte[4]

Abstract: Soil-structure interaction may play a major role in the seismic response of a bridge structure. Specifically, soil layers of low stiffness and strength may result in permanent displacement of the abutments and foundations, thus imposing important kinematic conditions to the bridge structure. A study to illustrate such phenomena is undertaken based on three-dimensional nonlinear dynamic finite-element (FE) modeling and analysis (for a specific bridge configuration under a given seismic excitation). A bridge-foundation-ground model is developed based on the structural configuration and local soil conditions of the Humboldt Bay Middle Channel Bridge. The FE model and nonlinear solution strategy are built in the open-source software platform OpenSees of the Pacific Earthquake Engineering Research Center. Based on the simulation results, the overall system seismic response behavior is examined, as well as local deformations/stresses at selected critical locations. It is shown that permanent ground deformation may induce settlement and longitudinal/transversal displacements of the abutments and deep foundations. The relatively massive approach ramps may also contribute to this simulated damage condition, which imposes large stresses on the bridge foundations, supporting piers, and superstructure.

DOI: 10.1061/(ASCE)0733-9445(2008)134:7(1165)

CE Database subject headings: Bridges; Finite element method; Soil-structure interaction; Abutments; Seismic effects; Seismic analysis; California.

Introduction

Seismically induced ground deformation effects on foundations and structures continue to be a major concern. During the Hokkaido-Nansei-Oki, Japan earthquake (July 12, 1993), the most common patterns of damage to bridges were caused by ground failures such as liquefaction and lateral displacement (Yanev 1993). Similar observations were reported after other recent events including the 1989 Loma Prieta Earthquake (Baldwin and Sitar 1991; Seed et al. 1990) and the 1995 Kobe Earthquake (Sitar 1995; JGS 1996, 1998).

The three-dimensional (3D) nature of nonlinear bridge/soil response imposes significant computational challenges. For instance:

1. The spatial extent of the bridge-foundation-ground system is large, typically in the hundreds or thousands of meters, necessitating an appropriate finite-element (FE) mesh to provide adequate modeling resolution. Preprocessing and output visualization in 3D FE analysis can be quite tedious and time consuming;
2. In view of the highly nonlinear properties of the foundation soil, elaborate hysteretic constitutive models of soil materials are needed, in a time-domain solution, with many thousands of time steps and iterations; and
3. Spatial definition of the input seismic excitation and soil boundary conditions remain an area of ongoing research.

These challenges impose high demands on software efficiency and hardware performance (e.g., high speed CPU, and large memory). Nevertheless, recent efforts on 3D modeling and analysis of structure-ground systems are being reported in the literature (e.g., Casciati and Borja 2004; Ju 2004; Jeremic et al. 2004; Yang and Jeremic 2005).

Building on prior 2D modeling and simulation studies (Conte et al. 2002; Zhang et al. 2003, 2005), a pilot 3D FE modeling effort is presented in this paper for nonlinear seismic response analysis of a bridge-foundation-ground system. The modeling applies to a virtual bridge-foundation-ground system inspired from the Pacific Earthquake Engineering Research (PEER) Center Humboldt Bay Middle Channel Bridge (HBB) Testbed (Porter 2003, ⟨http://www.peertestbeds.net/humboldt.htm⟩). Thus, some key features of the actual bridge are not modeled (e.g., spliced regions at the base of the piers), and therefore the associated response mechanisms may not be captured by the present model.

The first part of the paper describes the bridge model characteristics along with the underlying foundation and ground properties. Thereafter the simulation results and potential scenarios of detrimental kinematic constraints imposed by the inelastic ground deformations are presented and discussed in the second part of the paper.

[1]Professor, Dept. of Structural Engineering, Univ. of California, San Diego, 9500 Gilman Dr., La Jolla, CA 92093 (corresponding author). E-mail: elgamal@ucsd.edu

[2]Senior Engineer, Saiful/Bouquet Consulting Inc., 385 E. Colorado Blvd., Suite 200, Pasadena, CA 91101. E-mail: james.linjun.yan@gmail.com

[3]Geotechnical Engineer, URS Corporation, 1333 Broadway, Suite 800, Oakland, CA 94612. E-mail: yangaaa@gmail.com

[4]Professor, Dept. of Structural Engineering, Univ. of California, San Diego, 9500 Gilman Dr., La Jolla, CA 92093. E-mail: jpconte@ucsd.edu

Note. Associate Editor: Reginald DesRoches. Discussion open until December 1, 2008. Separate discussions must be submitted for individual papers. To extend the closing date by one month, a written request must be filed with the ASCE Managing Editor. The manuscript for this paper was submitted for review and possible publication on March 6, 2006; approved on November 7, 2007. This paper is part of the ***Journal of Structural Engineering***, Vol. 134, No. 7, July 1, 2008. ©ASCE, ISSN 0733-9445/2008/7-1165–1176/$25.00.

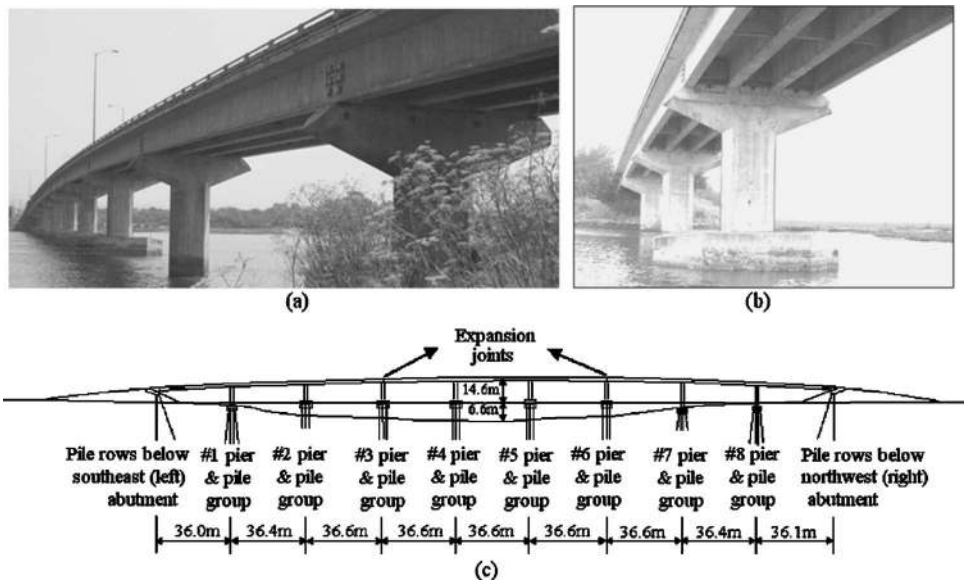

Fig. 1. Humboldt Bay Middle Channel Bridge (HBB): (a) overview, (b) closeup photo; and (c) global elevation view of bridge superstructure, piers, and foundation system

PEER Humboldt Bay Middle Channel Bridge Testbed

The HBB (Fig. 1) is 330 m long, 10 m wide, and 12 m high (average height over mean water level). The nine span superstructure consists of four precast prestressed concrete I-girders and cast-in-place concrete slabs. The I-girders are supported on the cap beams of single pier bents with both longitudinal and transversal shear keys to prevent unseating. Two expansion joints are located at the top of Piers 3 and 6 as shown in Fig. 1(c). The abutments and piers are supported on pile-group foundations [Fig. 1(c)].

Three of the eight pile-group foundations [1, 7, and 8 in Fig. 1(c)] consist of a 3.5×4 m pile-group with four interior vertical square piles (0.356 m/14 in.) and 12 exterior batter square piles (0.356 m/14 in.), and a 1.22 m thick pile cap below ground surface. The remaining five pile groups [2–6 in Fig. 1(c)], 3.5×5 m in size, are composed of five vertical circular piles (1.37 m/54 in. diameter) and a 1.53 m thick pile cap above ground. Each bridge abutment (1.2×10 m in size) is supported on two rows of circular piles ((0.356 m/14 in.) diameter), with seven front batter piles and five rear vertical piles [Fig. 1(c)].

The average slope of the river channel from the banks to its center is about 7% (4°). The foundation soil is composed mainly of dense fine-to-medium sand, organic silt, and stiff clay layers. Thin layers of loose and soft clay are located near the ground surface. With no laboratory stress-strain data available for soils at this site, definition of pressure dependent soil modeling parameters is deemed an unnecessarily complex undertaking. Rather, focus is maintained on capturing the key nonlinear dynamic hysteretic characteristics of soil response. In addition, with pressure dependence and a solid-fluid coupled formulation, in-core execution of computations on a single Personal Computer would have been virtually impossible. As such, resort to a 3D pressure-independent hysteretic soil modeling procedure was the selected path forward.

Finite-Element Analysis Framework/Platform: OpenSees

System modeling and response computations are performed using OpenSees, an object-oriented, open-source FE analysis framework (McKenna 1997; McKenna and Fenves 2001). In the bridge-foundation-ground model, different types of elements are employed to represent the foundation, piers and superstructure such as: (1) 3D linear elastic beam-column element; (2) 3D fiber-section force-based beam-column element (Spacone et al. 1996; De Sousa 2000; McKenna and Fenves 2001) with nonlinear fiber materials (in practice, fiber-section modeling may be handled by computer codes such as XTRACT ⟨http://www.imbsen.com/xtract⟩); (3) Four-node linear elastic shell element (MITC4, Bathe 1996); (4) Hexahedra solid element (eight-node brick, Bathe 1996); and (5) Linear ZeroLength element (McKenna and Fenves 2001) connecting two coincident nodes with linear elastic translational/rotational springs.

Finite-Element Model

Generally, effort is directed towards: (1) inclusion of a representative soil domain around the bridge structure; and (2) investigation of the resulting soil-structure interaction/deformation effects. The 3D mesh of this bridge-foundation-ground system (Fig. 2) is generated and visualized using the pre/postprocessor software GiD (Diaz and Amat 1999). This FE model (Fig. 2) includes 30,237 nodes, 1,140/280 linear/nonlinear beam-column elements, 81 linear shell elements, 23,556 nonlinear solid brick elements, 1,806 linear zero-length elements, and 2,613 equal degree of freedom (DOF) constraints (McKenna and Fenves 2001). The soil domain represented in this computational model is 650 m long, 151 m wide, and 74.5 m deep.

Bridge Superstructure

The main longitudinal bridge I-girders ($A=0.73$ m^2, $I_z=0.49$ m^4, and $I_y=0.0094$ m^4) and transversal brace I-beams ($A=0.1$ m^2,

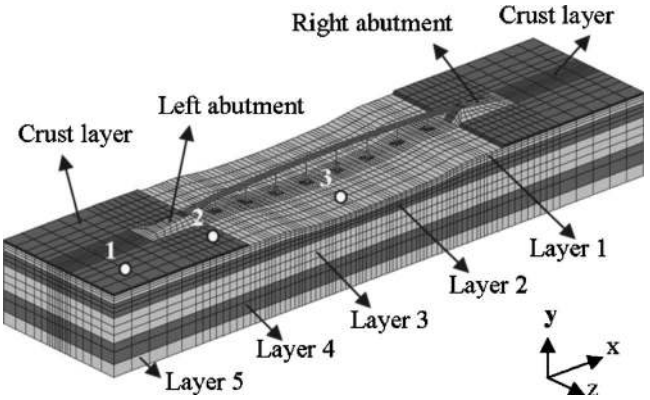

Fig. 2. 3D FE model of bridge and idealized soil profile

I_z=0.067 m^4, and I_y=0.00017 m^4) are modeled using 3D linear elastic beam-column elements. The bridge deck slab (0.165 m thick) is modeled using 3D linear elastic shell elements. In this study, the following concrete material properties are used (Wang and Salmon 1992): mass density ρ=2,300 kg/m^3, compressive strength f'_c=5 ksi, Young's modulus $E=2.78\times10^7$ kPa (corresponding to f'_c=5 ksi), and Poisson's ratio ν=0.3 of concrete are used.

In order to model the presence of expansion joints above the third and sixth piers, the bridge deck is subdivided into three continuous subsections. In the present model, these sections are simply connected by perfect hinges using the equalDOF constraint (for the three translations only) in OpenSees (McKenna and Fenves 2001). As such, a perfect hinge dictates equal translations, with no constraint on all rotations.

Table 1. Constitutive Model Parameters [Fig. 3(c)] for Concrete Material Used in Fiber Beam-Column Element

Concrete material model in OpenSees	Confined concrete	Unconfined concrete
Compressive strength f'_c (kPa)	-3.45×10^4 (−5 ksi)	-2.76×10^4 (−4 ksi)
Strain at compressive strength (ε_c)	−0.004	−0.002
Crushing strength f_{cu} (kPa)	-2.07×10^4 (−3 ksi)	0 —
Strain at crushing strength (ε_{cu})	−0.014	−0.008

Bridge Piers

The bridge piers are modeled using 3D fiber-section force-based beam-column elements with nonlinear fiber materials. Discretization of the pier cross section into concrete and steel fibers is shown in Fig. 3(a), with confined and unconfined concrete inside and outside the shear reinforcement/stirrups, respectively. The uniaxial Kent–Scott–Park model (Kent and Park 1971; Scott et al. 1982; Mander et al. 1988) with degraded linear unloading/reloading stiffness [Fig. 3(c)] is used to model the concrete (Table 1). The reinforcing steel is represented by a uniaxial bilinear inelastic model with kinematic hardening (equivalent to the 1D J_2 plasticity model with linear kinematic and no isotropic hardening) as shown in Fig. 3(d), with the following material parameters: yield strength $f_y=4.14\times10^5$ kPa (60 ksi), Young's modulus $E_s=2\times10^8$ kPa (29,000 ksi), and strain hardening ratio b=0.008. Compared to the confined concrete (Table 1), the unconfined concrete material is characterized by a lower compressive strength, lower crushing strength, and lower strain ductility. Figs. 3(e and f) show the cyclic moment-curvature response of the cross section

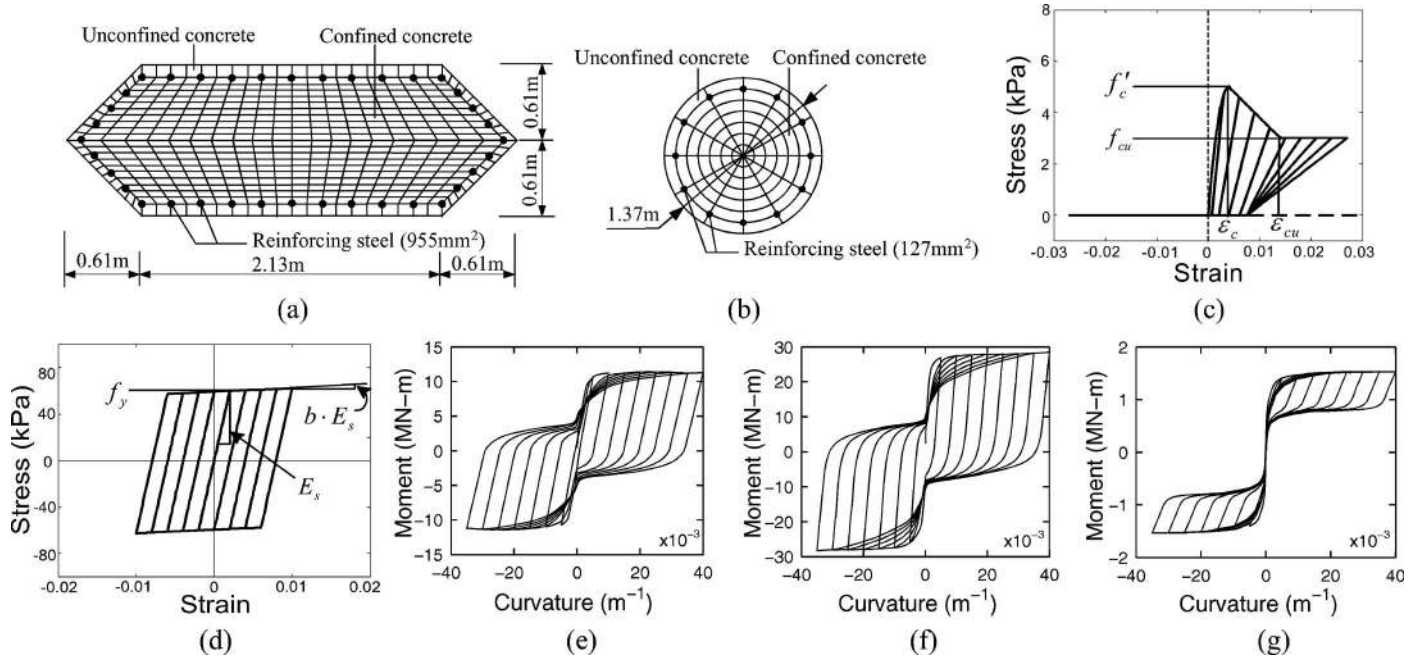

Fig. 3. Modeling of pier and pile group using fiber-section beam-column element with uniaxial material constitutive models: (a) fiber discretization of pier cross section; (b) fiber discretization of pile cross section; (c) concrete Kent–Scott–Park model with degraded linear unloading/reloading stiffness; (d) reinforcing steel bilinear inelastic model with linear kinematic hardening; (e) cyclic moment-curvature response of pier cross section for longitudinal bending; (f) cyclic moment-curvature response of pier cross section for transversal bending; and (g) cyclic moment-curvature response of circular pile cross section

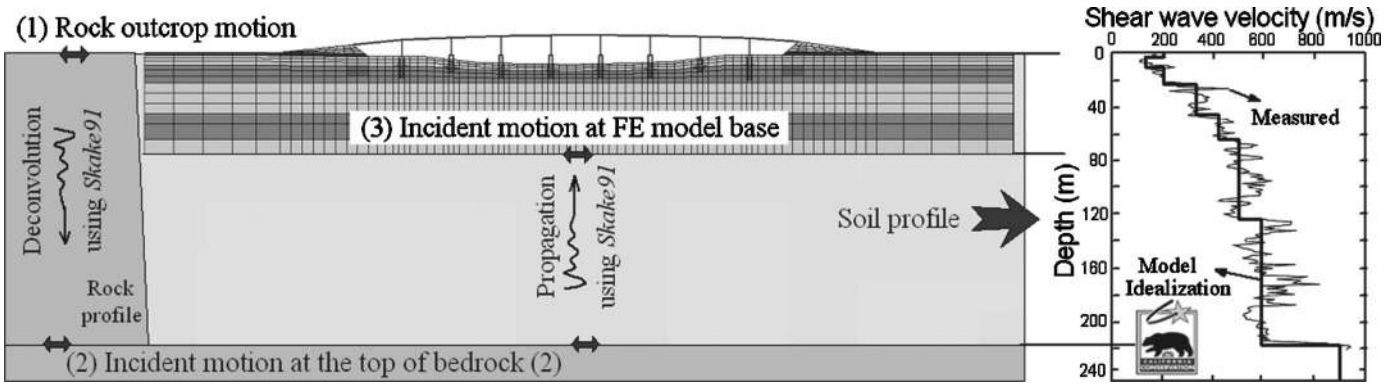

Fig. 4. Deconvolution of rock outcrop motion using Shake91 (Idriss and Sun 1993), along with idealized and measured soil shear wave velocity profile (adapted from CGS/SMIP CSMIP Station No. 89734)

of the bridge piers under an axial load of 8 MN ($\cong 0.08 f'_c A_g$, where A_g denotes the gross cross-section area) representative of the action of gravity. It is seen that the pier has a much higher flexural capacity in the transversal direction (28 MN m) than in the longitudinal direction (11 MN m).

Quasi-rigid elements (linear beam-column elements with Young's modulus of 3.0×10^{10} kPa and a square cross-sectional area of 4 m^2) are used to model the pier cap beams assumed herein to be of adequate strength and high stiffness. The bridge superstructure is connected to the cap beams through perfect hinges using the equalDOF constraint (for the three translations only) in OpenSees (McKenna and Fenves 2001), assuming no shear key failure.

Pile Groups

As mentioned earlier, the bridge piers are supported on pile foundations [Fig. 1(c)], each consisting of 16 square piles (Piers 1, 7, and 8) or five circular piles (Piers 2–6). In the FE model, in order to reduce the complexity of 3D mesh generation, 2×2 pile groups are employed throughout, with four vertical piles. To represent the spatial configuration, both the longitudinal and transversal spacing for pile Groups 1, 7, and 8 [Fig. 1(c)] are 2.67 m on center (o.c.). As for pile Groups 2–6 [Fig. 1(c)], the pile spacing is 2.67 m (o.c.) longitudinally and 4 m (o.c.) transversally.

Each pile is modeled using 3D fiber section, force-based beam-column elements with the same nonlinear fiber materials as for the piers [Fig. 3(b)]. Below ground, rigid beam-column links, normal to the pile longitudinal axis, are used to represent the geometric space occupied by each pile. The soil domain 3D brick elements are connected to the pile geometric configuration at the outer nodes of these rigid links using the equalDOF constraint in OpenSees for translations only (Yan 2006).

Fig. 3(g) shows the cyclic moment-curvature response of this circular pile cross section under a constant axial load of 2 MN ($\cong 0.04 f'_c A_g$) representative of the action of gravity. Because the pile is circular, it has the same flexural capacity (1.5 MN m) in the longitudinal and transversal directions.

Modeling of the pile caps depended on the location. The pile caps above ground [2–6 in Fig. 1(c)] are idealized as rigid frames, and the inertial properties of these massive pile caps are represented by a lumped mass of 33×10^3 kg at each of the four corner nodes. The pile caps below ground surface [1, 7, 8 in Fig. 1(c)] are modeled by a layer of solid elements (with linear elastic properties corresponding to uncracked concrete) to represent the actual geometric configuration.

Abutments and Soil Domain

Fig. 4 shows the employed idealized shear wave velocity profile of the underlying soil. This profile is defined according to field data (also shown in Fig. 4) measured by *OYO* suspension logging at Borehole 1 of the Caltrans Samoa Bridge Geotechnical downhole array, about 0.4 km north-west of the HBB (C. Roblee, personal communication, 2002).

As shown in Fig. 2, the soil profile is idealized into a surface crust layer, and five underlying sublayers (Table 2). Layer 1 (Fig. 2) varies in thickness from 4.9 m at the center of the river channel to 7.3 m at the banks. This layer is modeled as a relatively soft soil material in order to study the effects of lateral soil displacement on the bridge foundation and superstructure (typical situation of a river deposited soft stratum). Shear strength of this soft layer is defined as 10 kPa, a representative value for young San Francisco Bay mud (Bonaparte and Mitchell 1979; Goldman 1969; Rogers and Figuers 1991).

The stiffness and strength of the soft soil layer are increased locally (to 25 kPa) below the bridge abutments and approach ramps in order to support the imposed relatively high vertical stresses at this location. In addition, the abutment and supporting piles are represented by a block of linear (elastic) 3D solid elements (mass density=2,100 kg/m^3, $E=5 \times 10^5$ kPa, $\nu=0.25$) representative of the original pile-soil system stiffness, so as to reduce the FE model complexity (Yan 2006). The abutment slope towards the river channel is 40°, and the approach ramp average side slope is 30° (Fig. 2). In the present model, the bridge superstructure is connected to the abutments through perfect hinges using equalDOF constraints (for the three translations only) in

Table 2. Soil Layer Properties

Soil layer in Fig. 2	Mass density (kg/m^3)	Shear modulus G (kPa)	Poisson's ratio	Shear strength S_u (kPa)
Abutment soil	2,000	30,000	0.4	30
Crust layer	1,500	60,000	0.4	40
Crust layer below abutments	1,500	25,000	0.4	25
Layer 1	1,300	19,000	0.4	10
Layer 2	1,500	60,000	0.4	40
Layer 3	1,800	196,000	0.4	75
Layer 4	1,900	335,000	0.4	75
Layer 5	1,900	475,000	0.4	75

OpenSees (McKenna and Fenves 2001). More refined modeling of this important bridge component could potentially provide additional useful insights.

The foundation soil is modeled as a nonlinear hysteretic material (Prevost 1978; Parra 1996) with a Von Mises multisurface (Iwan 1967; Mroz 1967) kinematic plasticity model (PressureIndependMultiYield model in OpenSees). In this regard, focus is on reproduction of the soil hysteretic elastoplastic shear response (including permanent deformation). In this model, the nonlinear shear stress-strain backbone curve is represented by a hyperbolic relation (Kondner 1963) defined by two material constants: low-strain shear modulus and ultimate shear strength (Table 2).

Selection of the shear strength properties (Table 2) is based on the guidelines of Duncan et al. (1989). The resulting hysteretic behavior may somewhat overestimate damping during seismic excitation (Pyke 1979). However, in the current state of overall numerical model developments, and in light of the absence of actual soil behavior data, the selected soil model provides a convenient way of capturing the characteristics of potential permanent soil shear deformations that would adversely affect the bridge superstructure.

Boundary Conditions

Recent work (domain reduction method) is increasingly allowing for more accurate simulation of the 3D seismic wave propagation problem, and associated soil-structure interaction scenarios (e.g., Bielak et al. 2003, and Yoshimura et al. 2003). Below, a more traditional approach is employed. More insights can be gained in the future based on inclusion of approaches such as the domain reduction method (or by inclusion of other wave absorbing boundary conditions) within the overall analysis framework.

Lateral Mesh Boundaries

Near the ground surface, the soil response to seismic excitation is assumed to be predominantly caused by vertically propagating shear waves (e.g., Idriss and Sun 1993; Elgamal et al. 1995; Kramer 1996). Thus, in the free field (away from the bridge), the lateral response of the soil domain is expected to match closely that of a conventional shear beam (Kramer 1996). In this regard, the longitudinal/transversal mesh lateral boundaries with idealized identical soil profiles (Fig. 2) are constrained to undergo the same vertical and longitudinal/transversal motions, using the equalDOF constraint in OpenSees. These lateral boundaries are located as far as possible from the bridge so as to decrease any effect of these boundary conditions on the bridge response.

Along Model Base

For computational efficiency, it is desirable to limit the depth of the soil domain. In this study, the base of the computational soil domain is located at a depth of 74.5 m from the ground surface (Fig. 2), sufficiently far from the bridge foundations. Typically, during seismic excitation, soil strata below this depth can be represented by a transmitting boundary. In this study, the Lysmer–Kuhlemeyer (1969) boundary is applied along the base of the FE model so as to avoid spurious wave reflections along this model boundary. At each node along the base, three dashpots are activated in the x, y, and z directions, and the incident seismic wave excitation is defined by three dynamic equivalent nodal forces (details of this process are presented in Zhang et al. 2003, 2005, and Yan 2006).

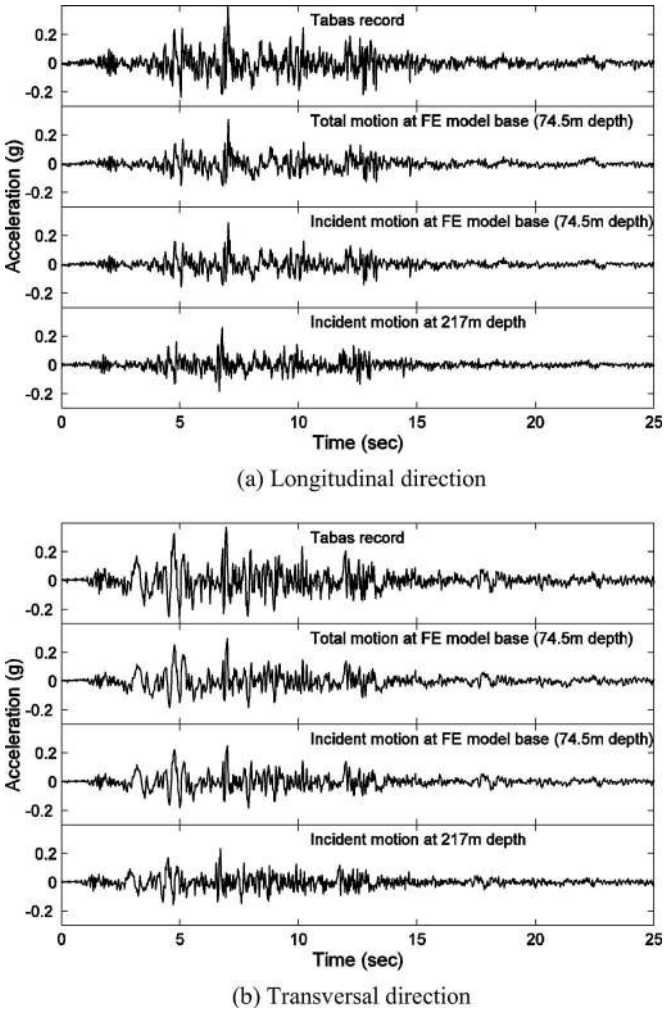

Fig. 5. Results of deconvolution: acceleration time histories of original rock outcrop motion (Location 1 in Fig. 4), bedrock incident motion (Location 2 in Fig. 4), and incident and total motion at FE model base (Location 3 in Fig. 4)

Definition of Input Excitation

As part of the research activities related to the PEER HBB testbed, the September 16, 1978 Tabas earthquake ground motion (Hartzell and Menodza 1991) was selected as a potential site-specific rock outcrop motion at a hazard level of 10% probability of exceedance in 50 years (Somerville and Collins 2002). This Tabas earthquake motion was then employed in this study to derive an incident earthquake motion along the base of the FE model (i.e., at a depth of 74.5 m) using the computer program Shake91 (Fig. 4, Idriss and Sun 1993; see Yan 2006 for details) to perform the deconvolution.

The deconvolution results obtained (Fig. 5) show that, in the longitudinal and transversal directions, the peak acceleration of the incident motion at the FE model base is 0.255g and 0.233g, respectively, compared to 0.439g and 0.373g peak ground acceleration in the original rock outcrop Tabas records. Finally, incident vertical motion at the FE model base (with a peak acceleration of 0.185g) is simply assumed to be half that of the original ground surface rock-outcrop vertical motion (Kramer 1996).

Solution Procedure

A staged analysis procedure is adopted with gravity loads applied first (statically) followed by dynamic earthquake excitation (Zhang et al. 2005, Yan 2006). Using this approach, 5,000 time steps ($\Delta t = 0.005$ s) of transient dynamic nonlinear analysis are executed to evaluate the system response during 25 s of earthquake excitation.

In the dynamic analysis phase, the incremental-iterative procedure used to integrate the equations of motion employed the Newmark-β time-stepping method with the time integration parameters $\gamma = 0.5$ and $\beta = 0.25$. In addition, the modified Newton–Raphson algorithm was adopted in order to avoid expensive calculations needed for the large number of DOFs. As such, the initial tangent stiffness (after application of gravity) of the system was used for all steps and iterations, and up to 20 iterations were needed for each step to achieve the prescribed tolerance (norm displacement increment less than 10^{-3}).

The large-scale FE model described above necessitated the use of a special sparse solver to allow in-core execution using a single personal computer (PC) with one 1.7 GHz CPU and 3 Gbytes of RAM. Major effort was expended in defining the geometric configuration of this large model (Fig. 2) in order to allow usage of a single PC (particularly in terms of number and size distribution of elements along the three spatial directions). The sparse solver was developed by Mackay et al. (1991) and Law and Mackay (1993) and implemented in OpenSees by Peng (2002). This solver is based on a row-oriented storage schema that takes full advantage of the sparsity of the stiffness matrix (Peng 2002). Using this solver, approximately, 40 h are needed for execution of the computations associated with the bridge-soil model of Fig. 2.

Seismic Response of Bridge-Foundation-Ground System

In the free field (e.g., Location 1 in Fig. 2), the horizontal ground surface response (Fig. 6) was found to be similar to that of a soil shear-column composed of the same nonlinear soil layers as the 3D FE model along the vertical line below Location 1 (Yan 2006). This indicates that the free-filed response of the defined mesh (with the employed input motion) is not greatly affected by the presence of bridge and river channels (it is important to note that no generalization for other input motion scenarios is implied by this observation).

Fig. 6 also compares the computed ground surface motion (acceleration time history) at three representative locations (1–3, indicated by white dots in Fig. 2) from the free field to the center of the river channel. In the vicinity of the center of the river channel center, higher peak accelerations and a larger frequency bandwidth are observed. It is also seen that the surface ground motion can change noticeably along the bridge spatial extent. Such a spatial variability of the surface ground motion may have some implications in simulation studies where the superstructure is studied without an underlying soil domain. Potential mechanisms behind this observed difference are discussed in the next section.

Figs. 7(a and b) show the residual deformation (elevation and plan views in exaggerated scale) of the entire bridge-foundation-ground system after earthquake shaking, where the arrows indicate the directions of soil flow, heave, settlement, and lateral displacement. Figs. 7(a–c) display computed damage scenarios such as settlement and tilting of the abutments, lateral displacement along the river bank, and the resulting deformation of the

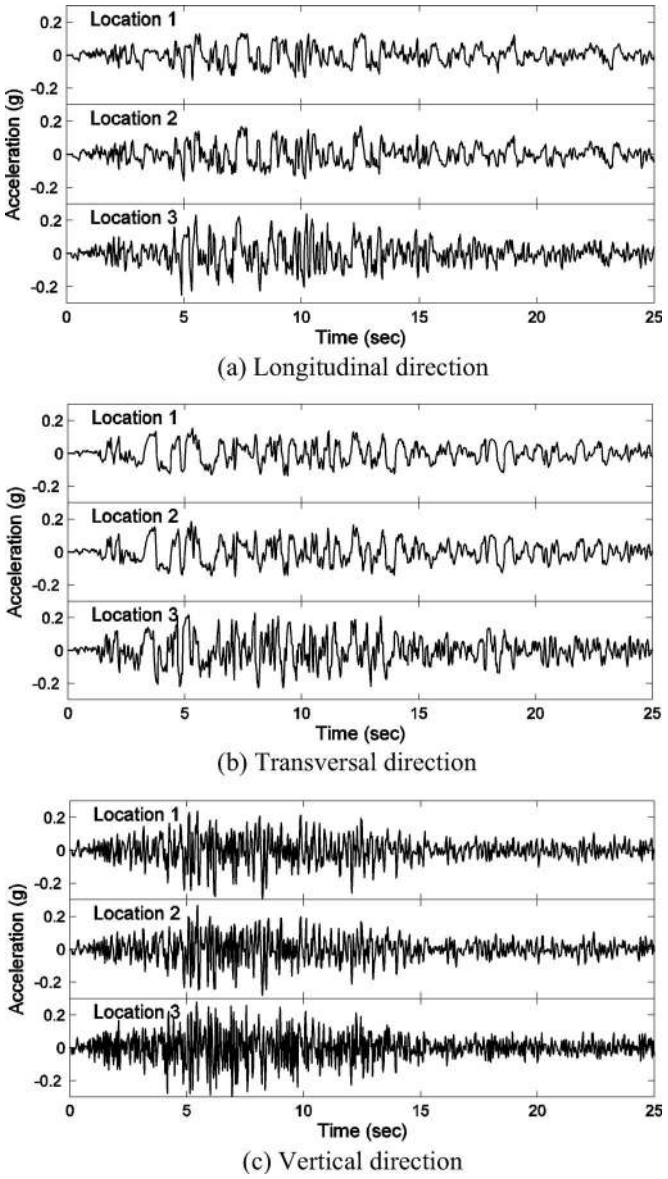

Fig. 6. Ground surface acceleration time history comparison for Locations 1–3 in Fig. 2

bridge foundation system and superstructure, which are reminiscent of past seismic damage to bridges [see Figs. 7(d and e)]. Superimposed on local deformations is a minor global lateral shift (0.04 m longitudinally and 0.05 m transversally) along the ground surface (upper 6 m), resulting from yielding in the underlying 4.9–7.3 m thick soft bay-mud layer.

Along the river banks [Figs. 7(a and b)], the yielded soil flows down slope towards the center of the river channel, and the maximum soil lateral movement at both river banks reaches approximately 0.28 m. Furthermore, the soil flowing towards the center of the channel elevates the river bed by about 0.1 m near the banks and about 0.05 m at the center [Fig. 7(a)].

The mass of the approach ramps results in settlement [Fig. 7(a) of about 0.3 m at the left abutment and 0.4 m at the right abutment]. Such large vertical settlement of the approach ramps would impede traffic and result in malfunction after the earthquake. Finally, Fig. 7(b) indicates transversal lateral displacement of the approach ramps (maximum of about 0.05 m), highlighting the 3D nature of soil deformation.

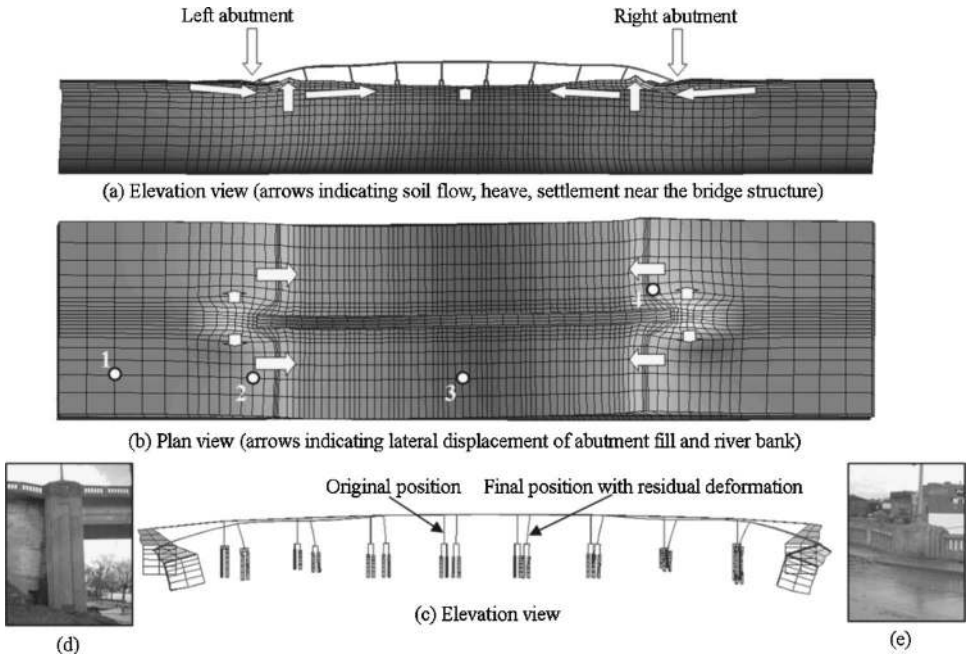

Fig. 7. Residual deformation of bridge-foundation-ground system after earthquake shaking (a–c) on exaggerated scale by a factor of 50; and similar damage scenarios observed in historical earthquake events (d–e) (Steinbrugge 2002)

Soil Response

Free Field Response

The soil shear stress-strain response at different depths below Location 1 on the ground surface [Figs. 2 and 7(b)] is shown in Fig. 8(a). Five different depths are considered: 1 m (middle of the crust layer), and 8, 20, 40, and 70 m (base of Layers 1, 2, 3, and 5). Near the base of the FE model (70 m depth), some yielding is observed at high shear stress levels, providing a sort of base isolation mechanism at this base soil layer. The bay-mud weak soil layer in the free field (top 8 m) experiences large inelastic deformations. Consequently, only low levels of shear stress are transmitted to the crust layer [see Fig. 8(a) at 1 m depth]. These low levels of shear stress in the surficial crust layer (free field) also correlate to the observed lower ground surface acceleration peaks at Location 1, as compared to Location 3 near the river channel center [Figs. 6(a and b)]. In this regard, inertial shear loads in the upper crust layer (which is only present in the free field) are limited by yielding in the underlying bay mud. This conclusion is further confirmed by results of separate studies (not presented here) based on 1D nonlinear shear column models with soil profiles corresponding to the free field (Location 1) and river channel center (Location 3) (Yan 2006).

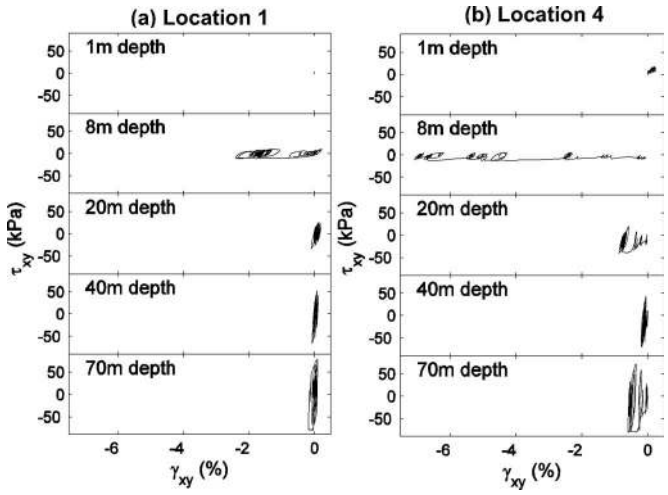

Fig. 8. Longitudinal (xy) shear stress-strain response at different depths below ground surface Locations 1 and 4 in Fig. 7(b)

Ground Response near Abutments

The soil shear stress-strain response at different depths below Location 4 on the ground surface near the right abutment [see Fig. 7(b)] is shown in Fig. 8(b). Compared to Fig. 8(a), much higher inelastic shear strains are observed in the 8–20 m depth range. The bridge approach ramp/abutment system near the channel slope has clearly induced additional soil deformations at this location compared to the free-field situation of Fig. 8(a). Additional locations around the left/right abutments are found to also display inelastic shear strains significantly larger than in the free field.

Response of Bridge Structure

Fig. 7(c) shows the elevation view of the permanent deformation (exaggerated by a factor of 50) of the bridge-foundation-ground system, including embankment soil and abutments, at the end of the earthquake. Soil lateral displacement causes the bridge pile groups to move towards the center of the river channel (maximum lateral permanent displacement of about 0.1 m at pile Group No. 1). The abutments have both settled (maximum of 0.21 m) and tilted (about 1°), resulting in significant levels of shear force and bending moment in the adjacent bridge girders (Yan 2006). Similar damage scenarios were observed in historical earthquake events [e.g., Rio Valdivia Bridge during the Chile 1960 Earthquake, Figs. 7(d and e), Steinbrugge (2002)].

It is observed in Fig. 7(b) that the permanent transversal displacement of the bridge is nonuniform ranging from 0.01 m (be-

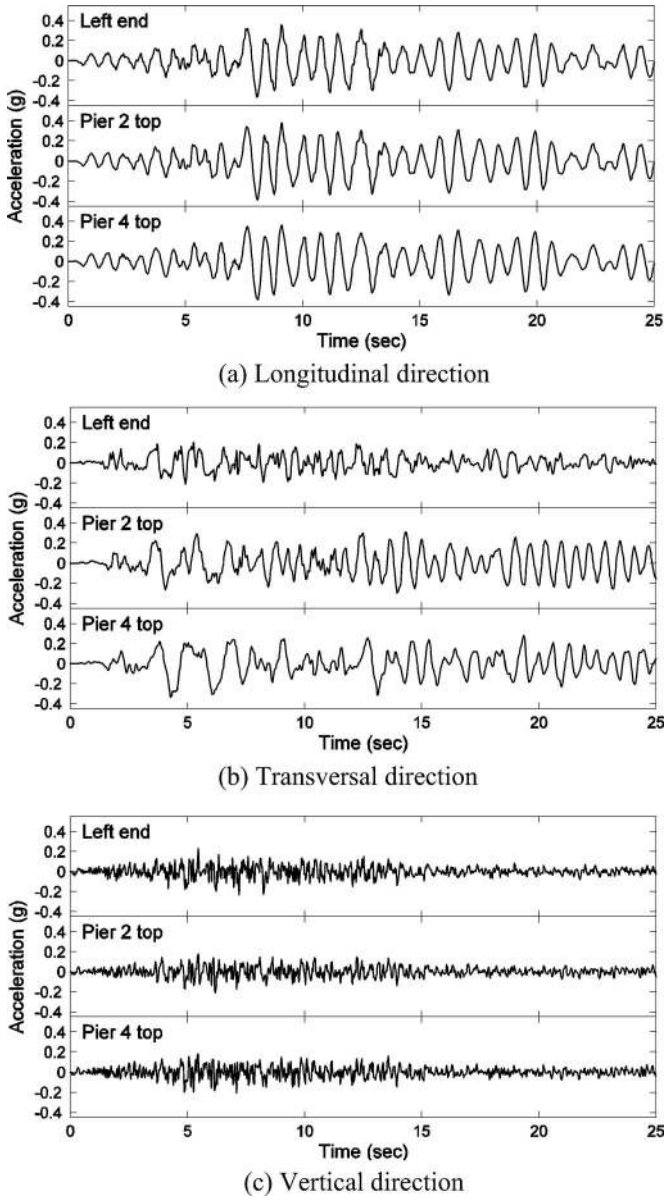

Fig. 9. Acceleration time histories at three locations along bridge superstructure

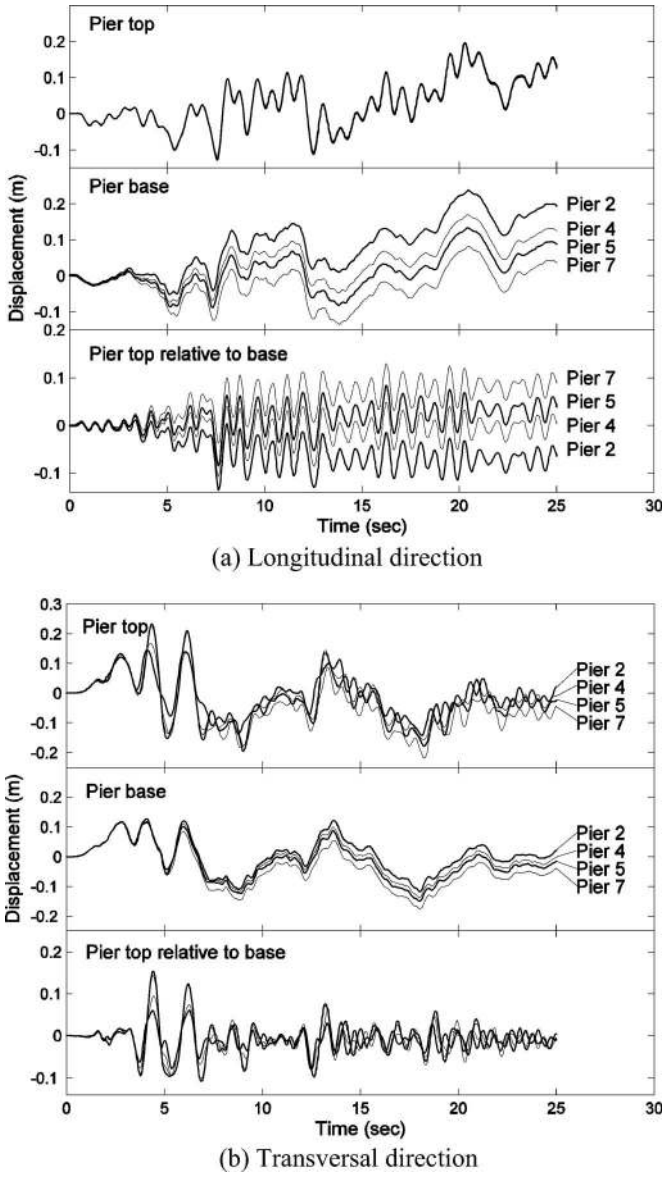

Fig. 10. Displacement time histories at bridge pier tops and bases

tween the first and second pile groups) to 0.12 m (near the right abutment). Generally, Figs. 7(a–c) highlight the significance of 3D analysis, and the inelastic ground deformation imposed on the bridge structure and its foundations.

Figs. 9(a–c) show acceleration time histories at three different locations along the bridge superstructure (left end, top of Pier 2, and top of Pier 4) in the longitudinal, transversal, and vertical directions, respectively. The longitudinal responses at these locations (with a clear 1.05 s period) are very similar due to the high axial stiffness of the superstructure [Fig. 9(a)]. The response of the bridge in the transverse direction is clearly amplified away from the bridge ends [Fig. 9(b)]. Compared to the pier base horizontal response (in the longitudinal and transversal directions), response at the pier tops is amplified and has a more narrow frequency content (i.e., the bridge structure acts as a filter).

Response of Bridge Piers

In the present model, the bridge deck subsystem is assumed linear elastic and is extremely stiff in the axial direction, maintaining the relative distance between the pier tops. However, spacing between the pile caps (at the pier bases) changed significantly due to soil migration towards the center of the river channel during the earthquake [Figs. 7(c) and 10(a)]. As might be expected, much lower levels of permanent deformation are observed in the transversal direction [Fig. 10(b)]. However, during earthquake excitation, the top-to-bottom relative displacement of the piers is still quite large (as large as in the longitudinal direction). This is a consequence of the relatively flexible transversal configuration of the bridge superstructure, in spite of the much higher moment of inertia of the piers cross section in this direction as compared to the longitudinal direction.

The relative top-to-bottom displacements of bridge piers induce large bending moments and shear forces. Since the bridge piers are fixed to the pile caps at the base and connected to the superstructure through shear keys (modeled as internal hinges), the maximum bending moment occurs at the base of each pier (Fig. 11). Fig. 11(a) shows the moment-curvature response and bending moment time histories in the pier base cross sections, in the longitudinal plane. In the outer piers (Piers Nos. 2 and 7),

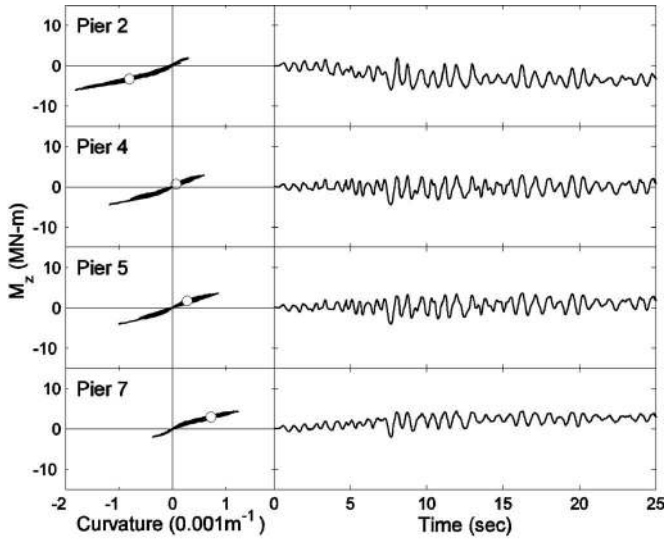

(a) Longitudinal direction

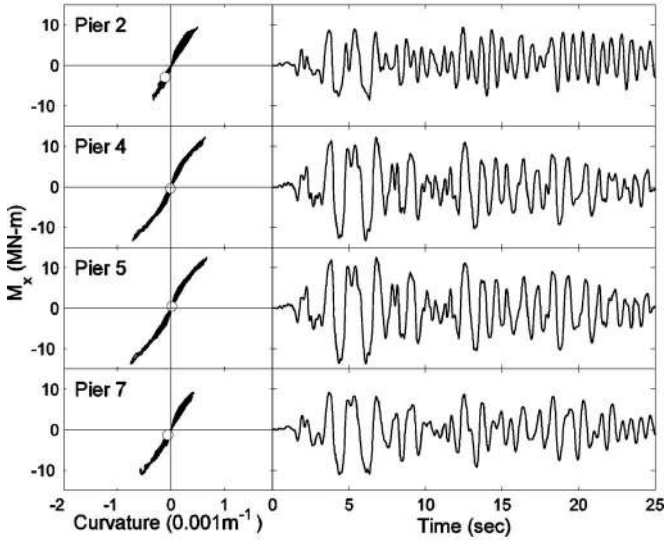

(b) Transversal direction

Fig. 11. Moment-curvature response and moment time histories at pier bases, with residual moment-curvature indicated by white dot

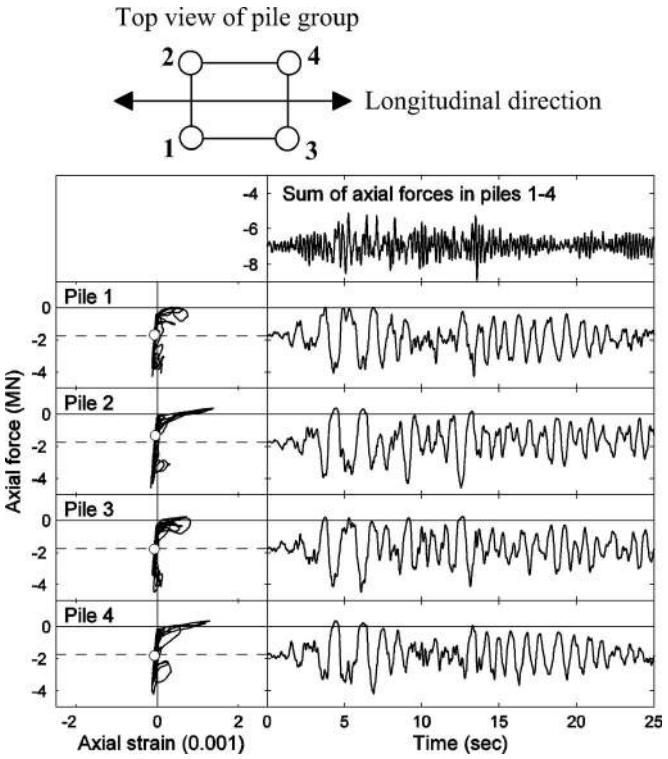

Fig. 12. Axial response of piles in Group 4: (1) diagram showing top view of pile group and numbering of piles; (2) axial force-average axial strain response and axial force time histories of each pile, with residual force strain indicated by white dot; and (3) sum of axial forces in all four piles

peak values exceeding 5 MN m [about 45% of the pier longitudinal bending moment capacity, Fig. 3(e)] are observed with significant residual moments due to soil lateral displacement, consistent with the overall permanent deformation response of the bridge-foundation-ground system [Fig. 7(c)]. From the moment-curvature response, a low level of nonlinearity (partial yield) is observed with the reinforcement steel unyielded and a minor (hair crack) level of damage in the concrete (Zhang et al. 2007).

The unrestrained cantilever-type transversal response of the bridge piers is driven by inertia effects and no significant residual moments and flexural deformations are observed [Fig. 11(b)]. The bending moment response in the transversal direction is about twice as high as in the longitudinal direction [Fig. 11(a)], with the peak moment reaching 15 MN m [about 50% of the pier transversal bending capacity, Fig. 3(f)]. However, the curvature response at the base of the piers is smaller in the transversal direction than in the longitudinal direction due to the significantly higher section bending stiffness in the transverse direction [Fig. 3(a)].

Response of Bridge Pile Foundations

Fig. 12 shows the axial force-average axial strain response and axial force time histories at the top of the four piles in Group 4. It is seen that the axial forces in all piles have significant fluctuation and the axial forces in the piles on the different sides of the bridge (Piles 1 and 3 versus Piles 2 and 4 in Fig. 12) vary in an opposite way. This is because during the earthquake, the cantilever configuration of the bridge superstructure in the transversal direction causes the pile caps to rock transversally, inducing opposite variations (increase/decrease) of the axial force in the piles on different sides of the bridge. The pile axial force time histories in Fig. 12 clearly exhibit a low frequency and narrow frequency bandwidth (single mode response) due to the pile cap rocking. These low frequency response components of individual piles cancel out as the axial forces of all four piles are summed up (see top-right corner of Fig. 12) to balance the axial force from the superposed pier and the vertical inertia force of the pile cap (which are characterized by a much higher frequency bandwidth).

Fig. 13 shows the axial force-average axial strain response and axial force time histories (at the top) of four single representative piles (with the same position of Pile 1 in Fig. 12) from Pile Groups 2, 4, 5, and 7, respectively. Figs. 12 and 13 show small tensile excursions of the axial force occurring in all piles, associated with a significant stiffness reduction. This marked change of stiffness reflects the lack of concrete participation (zero strength and zero stiffness) in tension, according to the material constitutive model adopted for concrete [Fig. 3(c)].

Fig. 14(a) shows the moment-curvature response in the longitudinal direction and moment time histories at the top of the same piles as in Fig. 13, with peak moment exceeding 1 MN m [2/3 of

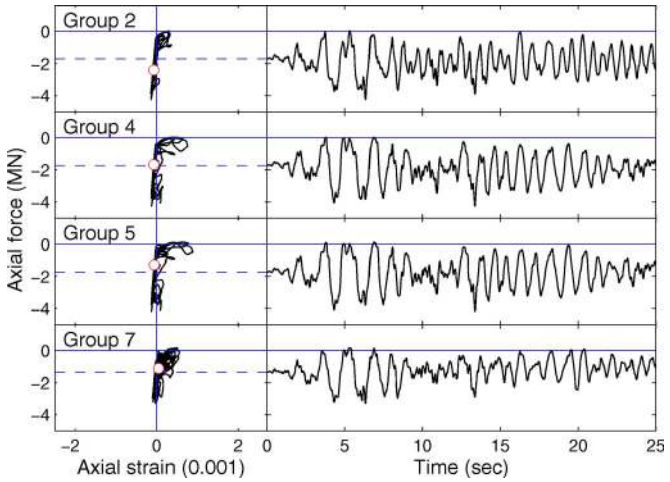

Fig. 13. Axial force-average axial strain response and axial force time histories at top of single representative piles (with same position of Pile 1 in Fig. 12), with residual force-strain indicated by white dot

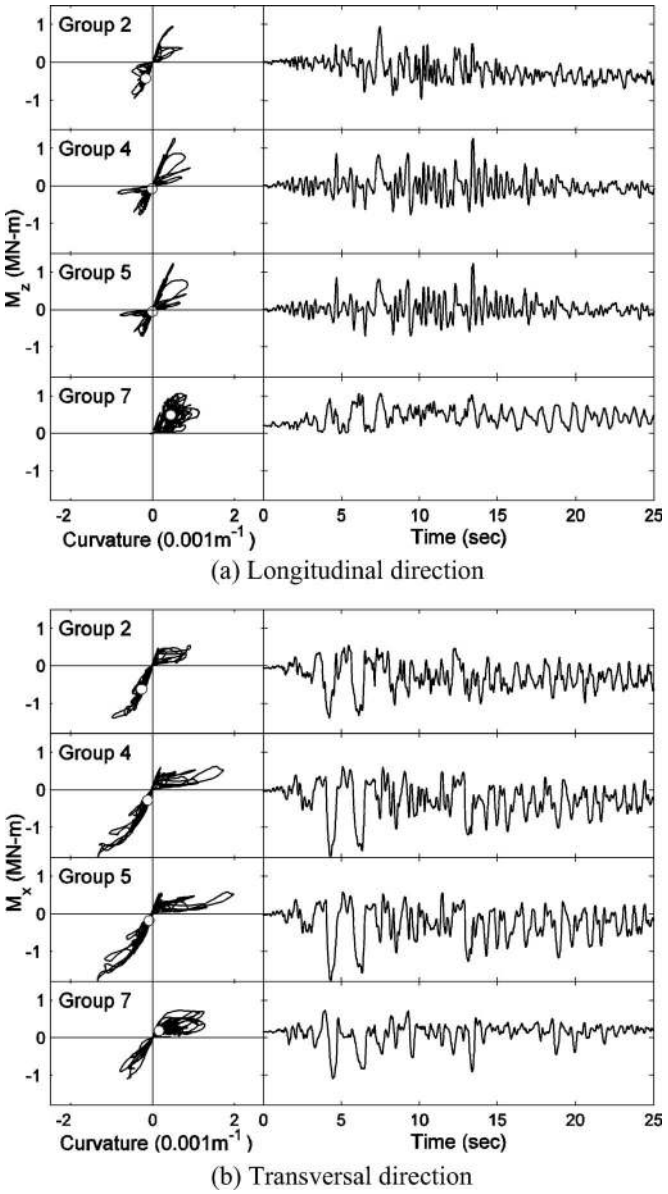

Fig. 14. Moment-curvature response and moment time histories at top of single representative piles (with same position of Pile 1 in Fig. 12), with residual moment-curvature indicated by white dot

the moment capacity of the pile, Fig. 3(g)]. Residual flexural deformations appear particularly in the outer pile groups (Nos. 2 and 7) consistent with the overall residual deformation pattern of the bridge [Fig. 7(c)]. For pile Group 7 with the pile cap embedded in the soil [Fig. 1(c)], moment in the representative pile does not change sign during the earthquake due to the lateral soil displacement towards the center of the river channel.

Fig. 14(b) shows moment-curvature response in the transversal direction and moment time histories at the top of the same four piles as in Figs. 13 and 14(a). For the single representative piles in pile Groups 4 and 5 (middle of the bridge), peak moments exceed 1.5 MN m and are near the flexural capacity of the piles [Fig. 3(g)]. The moment-curvature response exhibits significant nonlinearities and large flexural ductilities (ratio of maximum absolute curvature to effective yield curvature, Conte et al. 2002) in excess of 10.

As mentioned earlier, the axial force in each pile undergoes significant fluctuations due to rocking of the pile cap induced by the dynamic response of the bridge in the transversal direction (see Figs. 12 and 13). The pronounced asymmetric bending response of each pile in the transversal direction [Fig. 14(b)] is explained by the facts that: (1) the flexural capacity depends significantly on the axial force and (2) the axial force and transversal bending moment at the top of a given single pile reach their local maximum/minimum at the same time [see Figs. 13 and 14(b)]. In other words, during each cycle of rocking response in the transversal direction, a given pile section undergoes: (1) a local maximum bending (in one direction) and maximum compressive force (which increases the bending capacity), followed by (2) a local maximum bending (in the other direction) and minimum compressive force (which decreases the bending capacity). This pattern of response occurs within the upper 8 m or so of each pile where the axial force approaches the tensile state. Finally, it is noted that the pile flexural response in the longitudinal direction [Fig. 14(a)] also exhibits higher peak bending response at instances of higher compressive axial force.

Summary and Conclusions

In order to study the effect of seismically induced ground deformation on bridge system response, a 3D nonlinear FE bridge-foundation-ground model is developed, in light of the structural configuration and site seismicity of the PEER HBB testbed. In this model, the soil profile is idealized into a surface crust layer and five underlying sublayers, and the top sublayer is selected as a relatively soft material in order to study the effect of lateral inelastic ground deformation on the bridge foundation, piers, and superstructure. A staged nonlinear dynamic analysis procedure is adopted to evaluate the system seismic response. Among the main observations are:

1. Soil nonlinear response, and in particular the yield strength, can impose limits on the acceleration that can be transferred to the upper strata due to base-isolation effects;
2. Changes in properties of the upper surficial soil layers along the bridge length may dictate significantly different time histories of dynamic excitation at the various support points of the bridge (i.e., bases of piers and abutments);
3. Soil lateral deformation primarily towards the center of the

underlying river channel must be taken into consideration in order to determine the level of permanent (residual) displacements and corresponding internal forces in the bridge structure, especially in the piers and foundation piles, which are difficult to predict without modeling the soil domain explicitly;

4. In the longitudinal direction, the bridge structure may be subjected to significant residual loads due to the soil lateral deformation mechanism and its effects on the bridge foundations. The inertial effects of the abutments and approach ramps also play an important role in this response mechanism;
5. In the transversal direction, the cantilever configuration of the bridge superstructure induces significant dynamic loads that must be resisted by the bridge piers and underlying pile foundations. In particular, the outside piles of a pile group foundation may experience during the earthquake axial tensile force excursions that must be carefully assessed; and
6. Finally, the computed approach ramp deformations and abutment displacements are shown to permanently and significantly increase flexural forces in the bridge superstructure, and may potentially affect the bridge operability after the earthquake. In view of the high significance of the bridge-abutment interaction, a more accurate representation of the abutment and connectivity to the bridge structure would be most worthwhile.

Acknowledgments

Support of this work was provided by the Earthquake Engineering Research Centers Program of the National Science Foundation, under Award No. EEC-9701568 through the Pacific Earthquake Engineering Research Center (PEER). This support is gratefully acknowledged. The writers wish to thank Mr. Patrick Hipley, Dr. Cliff Roblee, Dr. Charles Sikorsky, Mr. Thomas Shantz, and Mr. Mark Yashinsky of Caltrans for providing all the requested information regarding the Humboldt Bay Middle Channel Bridge. Professor Gregory Fenves and Dr. Frank McKenna of U.C. Berkeley and Professor Michael Scott of Oregon State University helped with the OpenSees modeling and analysis phase. Professor Kincho Law and Dr. Jun Peng (Stanford University) were instrumental in providing their sparse solver and assisting in every way. This assistance was most valuable and is highly appreciated.

References

Baldwin, J. E., II, and Sitar, N., eds. (1991). "Loma Prieta Earthquake: Engineering geologic perspectives." *Special Publication No. 1*, Association of Engineering Geologists, San Francisco.

Bathe, K. J. (1996). *Finite element procedures*, Prentice-Hall, Upper Saddle River, N.J.

Bielak, J., Loukakis, K., Hisada, Y., and Yoshimura, C. (2003). "Domain reduction method for three-dimensional earthquake modeling in localized regions. Part I: Theory." *Bull. Seismol. Soc. Am.*, 93(2), 817–824.

Bonaparte, R., and Mitchell, J. K. (1979). *The properties of San Francisco Bay mud at Hamilton Air Force Base, California*, University of California Press, Berkeley, Calif.

Casciati, S., and Borja, R. I. (2004). "Dynamic FE analysis of South Memnon Colossus including 3D soil-foundation-structure interaction." *Comput. Struct.*, 82, 1719–1736.

Conte, J. P., Elgamal, A., Yang, Z., Zhang, Y., Acero, G., and Seible, F. (2002). "Nonlinear seismic analysis of a bridge ground system." *Proc., of 15th Engineering Mechanics Conf.*, ASCE, Reston, Va.

De Sousa, R. M. (2000). "Force-based finite element for large displacement inelastic analysis of frames." Ph.D. dissertation, Univ. of California, Berkeley, Calif.

Diaz, N. D., and Amat, P. S. (1999). *GiD the personal pre/postprocessor user's manual, version 5.0*, CIMNE, Barcelona, Spain, ⟨http://gid.cimne.upc.es⟩.

Duncan, J., Horz, R., and Yang, T. (1989). "Shear strength correlations for geotechnical engineering." *Rep.*, Dept. of Civil Engineering, Virginia Tech., Blacksburg, Va.

Elgamal, A., Zeghal, M., and Parra, E. (1995). "Identification and modeling of earthquake ground response." K. Ishihara, ed., Balkema, *Proc., 1st. Int. Conf. on Earthquake Geotechnical Engineering, IS-TOKYO'95*, Vol. 3, Tokyo, 1369–1406.

Goldman, H. B., ed. (1969). "Geologic and engineering aspects of San Francisco Bay fill." *Special Rep. No. 97*, California Division of Mines and Geology, Sacramento, Calif.

Hartzell, S. H., and Mendoza, C. (1991). "Application of an iterative least-squares waveform inversion of strong-motion and teleseismic records to the 1978 Tabas, Iran earthquake." *Bull. Seismol. Soc. Am.*, 81(2), 305-331.

Idriss, I. M., and Sun, J. I. (1993). *User's manual for SHAKE91: A computer program for conducting equivalent linear seismic response analyses of horizontally layered soil deposits*, Center for Geotechnical Modeling, Dept. of Civil and Environmental Engineering, University of California Press, Davis, Calif.

Iwan, W. D. (1967). "On a class of models for the yielding behavior of continuous and composite systems." *J. Appl. Mech.*, 34, 612–617.

Japanese Geotechnical Society (JGS). (1996). "Special issue on geotechnical aspects of the January, 17, 1995 Hyogoken-Nanbu earthquake." *Soils Found.*, 36(1), 1–359.

Japanese Geotechnical Society (JGS). (1998). "Special issue on geotechnical aspects of the January 17, 1995 Hyogoken-Nanbu Earthquake, No. 2." *Soils Found.*, 38(2), 1–216.

Jeremic, B., Kunnath, S., and Xiong, F. (2004). "Influence of soil-foundation-structure interaction on seismic response of the I-880 viaduct." *Eng. Struct.*, 26, 391–402.

Ju, S. H. (2004). "Three-dimensional analysis of wave barriers for reduction of train-induced vibrations." *J. Geotech. Geoenviron. Eng.*, 130(7), 740–748.

Kent, D. C., and Park, R. (1971). "Flexural members with confined concrete." *J. Struct. Div.*, 97(7), 1969–1990.

Kondner, R. L. (1963). "Hyperbolic stress-strain response: Cohesive soils." *J. Soil Mech. and Found. Div.*, 89(1), 115–143.

Kramer, S. L. (1996). *Geotechnical earthquake engineering*, Prentice-Hall, Englewood Cliffs, N.J.

Law, K. H., and Mackay, D. R. (1993). "A parallel row-oriented sparse solution method for finite element structural analysis." *Int. J. Numer. Methods Eng.*, 36, 2895–2919.

Lysmer, J., and Kuhlemeyer, R. L. (1969). "Finite dynamic model for infinite media." *J. Engrg. Mech. Div.*, 95(4), 859–877.

Mackay, D. R., Law, K. H., and Raefsky, A. (1991). "An implementation of a generalized sparse/profile finite element solution method." *Comput. Struct.*, 41, 723–737.

Mander, J. B., Priestley, M. J. N., and Park, R. (1988). "Theoretical stress-strain model for confined concrete." *J. Struct. Eng.*, 114(8), 1804–1826.

McKenna, F. T. (1997). "Object-oriented finite element programming: Frameworks for analysis, algorithms and parallel computing." Ph.D. dissertation, Univ. of California, Berkeley, Calif.

McKenna, F. T., and Fenves, G. L. (2001). *The OpenSees command language manual, Version 1.2*, Pacific Earthquake Engineering Research Center, Univ. of California, Berkeley, Calif.

Mroz, Z. (1967). "On the description of anisotropic work hardening." *J. ASTM Int.*, 15, 163–175.

Parra, E. (1996). "Numerical modeling of liquefaction and lateral ground deformation including cyclic mobility and dilation response in soil

systems." Ph.D. dissertation, Rensselaer Polytechnic Institute, Troy, N.Y.

Peng, J. (2002). "An internet-enabled software framework for the collaborative development of a structural analysis program." Ph.D. dissertation, Stanford Univ., Stanford, Calif.

Porter, K. A. (2003). "An overview of PEER's performance-based earthquake engineering methodology." *Proc., 9th Int. Conf. on Applications of Statistics and Probability in Civil Engineering (ICASP9)*, Civil Engineering Risk and Reliability Association (CERRA), San Francisco.

Prevost, J. H. (1978). "Plasticity theory for soil stress-strain behavior." *J. Engrg. Mech. Div.*, 104(5), 1177–1194.

Pyke, R. (1979). "Nonlinear soil models for irregular cyclic loadings." *J. Geotech. Engrg. Div.*, 105(6), 715–726.

Rogers, J. D., and Figuers, S. H. (1991). "Engineering geologic site characterization of the Greater Oakland-Alameda Area, Alameda and San Francisco Counties, California." *Rep.*, National Science Foundation, Washington, D.C.

Scott, B. D., Park, R., and Priestley, M. J. N. (1982). "Stress-strain behavior of concrete confined by overlapping hoops at low and high strain rates." *J. Am. Concr. Inst.*, 79(1), 13–27.

Seed, R. B., et al. (1990). "Preliminary report on the principal geotechnical aspects of the October 17, 1989 Loma Prieta Earthquake." *Rep. No. UCB/EERC-90/05*, Earthquake Engineering Research Center, Berkeley, Calif.

Sitar, N., ed. (1995). "Geotechnical reconnaissance of the effects of the January 17, 1995 Hyogoken-Nanbu Earthquake, Japan." *Rep. No. UCB/EERC-95/01*, Earthquake Engineering Research Center, Berkeley, Calif.

Somerville, P., and Collins, N. (2002). "Ground motion time histories for the Humboldt Bay Bridge." *Rep. Prepared for the PEER Methodology Testbeds Project*, URS Corporation, Pasadena, Calif.

Spacone, E., Filippou, F. C., and Taucer, F. F. (1996). "Fibre beam-column model for non-linear analysis of R/C frames. Part I: Formulation." *Earthquake Eng. Struct. Dyn.*, 25(7), 711–725.

Steinbrugge, K. V. (2002). *The Karl V. Steinbrugge slide and photograph collection World Earthquakes and Earthquake Engineering*, Earthquake Engineering Research Center, Berkeley, Calif., ⟨http://nisee.berkeley.edu/eqiis.html⟩.

Wang, C. K., and Salmon, C. G. (1992). *Reinforced concrete design*, 5th Ed., HarperCollins, New York.

Yan, L. (2006). "Sensor data analysis and information extraction for structural health monitoring." Ph.D. dissertation, Univ. of California, San Diego.

Yanev, P. (1993). "Hokkaido Nansei-Oki Earthquake of July 12, 1993." *EQE Review*, Fall, 1–6.

Yang, Z., and Jeremic, B. (2005). "Study of soil layering effects on lateral loading behavior of piles." *J. Geotech. Geoenviron. Eng.*, 131(6), 762–770.

Yoshimura, C., Bielak, J., Hisada, Y., and Fernández, A. (2003). "Domain reduction method for three-dimensional earthquake modeling in localized regions. Part II: Verification and applications." *Bull. Seismol. Soc. Am.*, 93(2), 825–840.

Zhang, Y., Conte, J. P., Yang, Z., Elgamal, A., Bielak, J., and Acero, G. (2008). "Two-dimensional nonlinear earthquake response analysis of a bridge-foundation-ground system." *Earthquake Spectra*, 24(2), May.

Zhang, Y., Yang, Z., Bielak, J., Conte, J. P., and Elgamal, A. (2003). "Treatment of seismic input and boundary conditions in nonlinear seismic analysis of a bridge ground system." *Proc., 16th Engineering Mechanics Conf.*, ASCE, Reston, Va.